Label-free biomarkers of human embryonic stem cell differentiation to hepatocytes

Label-free biomarkers of human embryonic stem cell differentiation to hepatocytes

Dimitrios Tsikritsis, Hu Shi, Yuan Wang, Srinivas Velugotla, Vlastimil Sršeň, Alistair Elfick and Andrew Downes.

Abstract

Four different label-free, minimally-invasive, live single cell analysis techniques were applied in a quantitative comparison, to characterize embryonic stem cells and the hepatocytes into which they were differentiated. Atomic Force Microscopy measures the cell's mechanical properties, Raman spectroscopy measures its chemical properties, and dielectrophoresis measures the membrane's capacitance. We were able to assign cell type of individual cells with accuracies of 91% (Atomic Force Microscopy), 95.5% (Raman spectroscopy), and 72% (Dielectrophoresis). In addition, Stimulated Raman Scattering (SRS) microscopy was able to easily identify hepatocytes in images by the presence of lipid droplets. These techniques, used either independently or in combination, offer label-free methods to study individual living cells. Although these minimally-invasive biomarkers can be applied to sense phenotypical or environmental changes to cells, these techniques have most potential in human stem cell therapies where the use of traditional biomarkers is best avoided. Destructive assays consume valuable stem cells and do not characterize the cells which go on to be used in therapies; whereas immuno-labelling risks altering cell behaviour. We suggest how these four minimally invasive methods can be applied to cell culture, and how they could in future be combined into one microfluidic chip for cell sorting.

Author information

Affiliations:

Institute for BioEngineering, University of Edinburgh, UK.

Dimitrios Tsikritsis, Hu Shi, Yuan Wang, Vlastimil Sršeň, Alistair Elfick and Andrew Downes.

School of Engineering, University of Glasgow, UK.

Srinivas Velugotla

Corresponding author:

Andrew Downes andy.downes@ed.ac.uk

Contributions:

A.D. designed research;

A.D. performed cell culture and differentiation;

A.D., D.T. and Y.W. acquired Raman spectra;

A.D. and H.S. performed atomic force microscopy;

A.D. and D.T. performed stimulated Raman scattering microscopy;

S.V. performed dielectrophoresis;

V.S. performed immunofluorescence;

A.D., D.T. and S.V. analyzed data;

A.D. and A.E. wrote the paper.

Competing financial interests:

There are no competing financial interests.

Acknowledgements

A.D. acknowledges funding from the Medical Research Council Grant G0802632. D.T. is supported by an EPSRC PhD studentship provided through the School of Engineering at the University of Edinburgh. All data used within this publication can be accessed at: http://dx.doi.org/10.7488/ds/317

Introduction

The non-destructive characterization of living cells is dominated by the use of biomarkers, namely fluorescent molecules (1,2) and more recently magnetic particles (3,4). However, we cannot rely on such tags to be non-invasive and have no effect on the cell's behaviour. Magnetic particles and fluorescent molecules are best suited to immunolabeling, where a membrane-specific antibody is attached to the label.

There are issues of phototoxicity of fluorescent molecules after the exposure to laser light required for imaging (5), and loading the membrane with antibodies is likely to influence the behaviour of the cell(6). Neither of these types of biomarkers can be relied upon to enter inside the cell membrane, so are limited in their observable changes in cell phenotype. Some cell types lack membrane-specific antibodies, in which case a label-free characterization technique is particularly attractive.

Human embryonic stem cells and induced pluripotent stem cells offer great potential in cell-based therapies and regenerative medicine (7,8), and in the pharmaceutical industry as a reliable source of human cells for drug testing (9,10). The dangers of teratoma formation (11,12) require an extremely careful selection and characterization of stem cells before clinical use. Regenerative medicine requires careful characterization of the cells which are used in therapies, as all the cells used in such therapies are required either (i) to retain their pluripotent or multipotent nature, or (ii) to be fully differentiated. However, traditional methods required for live single cell characterization such as antibody labeling are highly invasive as described above. All other methods are destructive, and usually 'sample' cells from within a larger culture population. This gives a clear advantage to an accurate live cell characterization technique which does not rely upon added biomarkers, and is minimally-invasive. Some cell features detected in white light imaging, such as cell size and shape,

and scattering of light, can be used to characterize cells. When combined, an accuracy of 96% was achieved when discriminating cancer cells from white blood cells(13). However, these cells are of different sizes so would be easy to distinguish based on morphology alone. When the same study investigated algal cells of more similar size but with different lipid content, they were distinguished with a reduced accuracy of 88%. The purpose of this study is to quantitatively compare four different label-free, non-destructive and minimally invasive methods of cell characterization, as potential clinical tools for quality control of individual stem cells and their differentiated progeny.

Atomic Force Microscopy (AFM)(14), depicted in Fig. S1, involves the use of a micromachined cantilever with a sharp tip at its end. In microscopy, the deflection of the cantilever is kept constant as the tip is raster-scanned across a surface. However, a cantilever can also be used to measure forces, without imaging. By pushing a sharp tip into a soft surface, some deformation of the cantilever occurs (bending upwards) and some deformation of the surface occurs. The relative proportions of these deformations is related to the elasticity (or Young's modulus) which is a material-specific quantity, not dependent on the size or shape of the cell.

AFM has previously been used to measure the elasticity of a variety of live cells(15), such as human embryonic stem cells (hESCs)(16), human amniotic fluid-derived stem cells (hAFSCs) against differentiated osteoblasts(17), and human mesenchymal stem cells (hMSCs) against differentiated osteoblasts(18). However, in none of these studies was an accuracy of assignment of cell type deduced. Nor has any AFM study been published on the directed differentiation of hESCs.

Raman spectroscopy(19) has been successfully applied to the label-free characterization of living cells. It uses laser spectroscopy to measure a vibrational spectrum of covalent bonds, each frequency being specific to part of a molecule (e.g. CH_2 groups in lipids, beta-sheet proteins, RNA).

The relative proportions of each of such chemistries gives rise to a 'fingerprint' spectrum specific to each cell type. So a cell phenotype change (such as disease) can be monitored on a single cell basis(20,21).

Raman spectroscopy has been applied to stem cells(22,23), and has monitored differentiation from adipose-derived stem cells (ADSCs) to osteoblasts (highlighting carbonate and phosphate mineralization, and collagen formation) and adipocytes (highlighting lipid droplet formation)(24). Caridomyocytes were differentiated from hESCs, and the two cell types identified with a sensitivity of 66%(25). The far higher sensitivities required for cell therapies have been achieved on hESCs versus cells which had undergone spontaneous differentiation(26). Raman spectroscopy has also been applied to monitoring the differentiation of embryonic stem cells toward cardiomyocytes, by comparing beating and non-beating embryoid bodies(27).

Raman microscopy – the acquisition of a Raman spectrum at each pixel of an image – is often too slow to be applied to high resolution imaging of living cells. More efficient versions of Raman microscopy which are fast enough to be applied to living cells, are coherent anti-Stokes Raman scattering (CARS) microscopy(28,29) and stimulated Raman scattering (SRS) microscopy(30,31). CARS microscopy images display signals which are quadratic with respect to concentration, and suffers from artefacts caused by optical interference with a constant signal known as the non-resonant background. SRS microscopy has neither of these problems, so produces images whose intensity is linear in concentration of the desired molecular bonds. CARS microscopy has previously been applied to monitoring the differentiation of adipose-derived stem cells(24,32) into both adipocytes (by imaging very large lipid droplets) and osteoblasts (by imaging nodules of phosphate).

Dielectrophoresis (DEP)(33) uses radio frequency electric fields to probe the high-frequency dielectric properties of living cells. These properties are dominated by capacitance of the cell membrane, which varies inversely with the membrane thickness. The other factor which affects the dielectrophoretic response is the area of the membrane. This is in turn dependent on cell diameter and shape, and membrane roughness. Dielectrophoresis can be used to characterize single cells in mixed populations (or average over large populations simultaneously), but it is also able to sort large numbers of cells – applying an electric field gradient at the right frequency produces a force gradient which causes one cell type to move in one direction, and the other cell type to move in the other direction(33).

DEP has been used to enrich the number of CD34+ cells (pluripotential hemopoietic stem cells) from peripheral blood stem cell harvest samples by a factor of 5(34), and has been used to characterize the differentiation of human embryonic stem cells into mesenchymal stem cells(35). DEP has also been employed to accurately characterize and sort murine neural stem / precursor cells (NSPCs) and their differentiated cells (neurons and glia)(36). More recently, DEP was exploited to characterize and sort terminally differentiated murine myotubes from multipotent C2C12 myoblasts to better than 96% purity(37).

We chose the differentiation of stem cells into hepatocytes for two main reasons. Firstly, mineralization or lipid droplets are trivial to spot in a Raman spectrum, and very stiff cells such as fibroblasts would be easy to distinguish from stem cells using AFM. So we selected a cell type which doesn't have a distinct chemical or mechanical fingerprint as a suitable challenge for the techniques. Secondly we wanted to choose a cell type which is clinically relevant, both to a prevalent condition – liver disease, and to a treatment via regenerative medicine – using scaffolds to create artificial tissue *ex vivo*, for implantation(38).

Materials and methods

Cell preparation

Human embryonic stem cells (RCM-1, UK Stem Cell Bank) were cultured in mTESR (Stemcell technologies) at 37 °C, 95% air, and 5% CO_2 in a humidified incubator without antibiotics. Culture flasks, glass-bottom dishes, and quartz substrates were coated with Matrigel (BD Biosceinces) diluted 32:1 in KO-DMEM (Invitrogen) overnight prior to seeding with cells. The Matrigel thickness has been measured as 10-20 μm(39). Cells were passaged 1:2 with a cell scraper to maintain colony structure. All experiments were performed on passage numbers in the range 75-85. Only when passage numbers rise above 120 will these embryonic stem cells start to lose their ability to self-renew and differentiate(40).

Efficient differentiation into hepatocytes was achieved following the protocol from Hay et al.(41) Briefly, differentiation was initiated for 3 days in RPMI1640 containing 1x B27 supplement (both from Invitrogen), 1 mM sodium butyrate (Sigma), 100 ng/ml ActivinA (Peprotech) and 50 ng/ml Wnt3a (R&D Systems). For the following 5 days, cells were cultured in media containing KO-DMEM (77.3%), KO-Serum Replacement (20%), Non-essential Amino Acids (1%), DMSO (1%), L-Glutamine (0.5%), and B-Mercaptoethanol (0.2%) (all from Invitrogen). For the last 9 days, cells were cultured in L15 medium (83%), fetal bovine serum (8.3%), tryptose phosphate broth (8.3%), 10 μM hydrocortisone 21-hemisuccinate, 1 μM insulin, 2 mM glutamine (all from Sigma); 10 ng/ml hepatocyte growth factor and 20 ng/ml oncostatin M (both from R&D systems).

Atomic Force Microscopy (AFM)

An AFM (Bioscope II, Bruker) was used on an inverted optical microscope (Nikon TE2000) with a 20x phase contrast objective lens (NA=0.5) in order to visualize cells and the AFM cantilever tip. Cells were investigated on glass-bottom dishes from within one hour of removal from the incubator.

RCM-1 cells were probed by MLCT-AUNM cantilevers (Bruker probes, nominal stiffness 0.01N/m, nominal radius 20 nm) in mTESR media, and differentiated hepatocytes were probed by MSNL cantilevers (Bruker probes, nominal stiffness 0.01N/m, nominal radius 2 nm) in 1x Phosphate Buffer Saline. The process of stiffness and elasticity measurement, illustrated in Fig. S1, is outlined as follows.

Firstly, the cantilever is indented into the glass substrate by a distance $Z_{apply} = Z_{tip}$. This produces a straight line graph of V (output voltage from quadrant photodiode) against Z_{tip}. The gradient of this graph, c, enables measurement of Z_{tip} from acquired values of V. The spring constant of the cantilever, k_{lever}, is calculated when the tip is far above the glass dish, by measuring the noise power spectrum of V. The total energy in this spectrum is equal to the thermal energy, k_BT. Three measurements of k_{lever} are averaged, and reveal less than 1% variation. This enables conversion of Z_{tip} into a measure of the force, F, at the end of the tip. The tip is then positioned above the centre of the cell nucleus, and a ramp of ~200 nm applied at 0.5 Hz. The indenting part of the curve is fitted to calculate elasticity, E, from the Hertz model of a sphere indenting a surface $F = 4/3.(E.R^{1/2}.\delta^{3/2}) / (1-v^2)$ where v is Poisson's ratio = 0.37 for biological tissues(42).***Raman Spectroscopy***

Raman spectra of individual living cells were acquired with 40 mW of 785 nm laser power, in an inverted microscope stage Raman spectrometer (Renishaw) and a 40x, NA 0.75, phase contrast objective lens – underfilled to an NA of around 0.25 to create a larger focal spot to minimize the possibility of photodamage. Spectra were acquired on cells (with the laser spot illuminating both nucleus and cytoplasm) for 8 acquisitions of 300 secs. A 'background' spectrum, dominated by the quartz substrate, was acquired beside the colony then subtracted from the cell's spectrum.

Raman spectra were automatically processed by several Matlab routines. The first of these removed the broad cellular autofluorescence by flattening the curves with a baseline subtraction Matlab

routine generously provided by H. Georg Schulze(43). Spikes in the spectrum caused by cosmic rays incident on the CCD spectrometer, were then found and removed using the Matlab routine generously provided by H. Georg Schulze(44). After this, all spectra were flattened again – in case the presence of cosmic rays affected the flattening process – then each spectrum was normalized in intensity. The processed spectra were then entered into the Matlab principal component analysis (PCA) routine. Each spectrum can be deconvolved into a linear combination of other principal component spectra, α.PC1 + β.PC2 + γ.PC3… , and coefficients (also known as scores) α, β, γ… were plotted on a scatter plot, for the two principal components which offered the greatest separation of the two groups of cells.

Dielectrophoresis (DEP)

RCM-1 embryonic cells and differentiated hepatocytes were centrifuged (100 x *g*, 5 minutes) and washed twice in 10 mL of the DEP medium, before final suspension in this medium at a density of ~10^7 cells/mL. The DEP isotonic medium consisted of 8.5% (w/w) sucrose, 0.5% (w/w) glucose, at pH 7.4 (adjusted with NaOH) and the conductivity was adjusted to 33 mS/m with culture medium. Osmolality (310 mOsm) and conductivity values were measured using an osmometer (Advanced Instruments Inc., Model 3300) and a conductivity meter (Oakton CON 510), respectively. The diameter of each cell in solution was measured with white light microscopy, and a high frequency electric field applied. The crossover frequency – at which the direction of movement of the cell reverses – is recorded for each cell.

Stimulated Raman Scattering (SRS) microscopy

We employed a home-built multi-photon microscopy system(45) adapted for SRS microscopy. This adaptation consists of the addition of an amplitude modulator (New Focus 4103-01) at 5 MHz to the

Stokes beam, and a lock-in amplifier (Stanford Research SR844) to the detection of transmitted pump beam.

We used 30 mW of each beam, measured at the sample, delivered by a water-immersion multi-photon objective lens (Olympus XLPlan N, NA 1.05, 25x). Stacks of 10 images were acquired at 1 μm separation, and converted into a 2-dimensional image by Z-projection at maximum intensity to observe all the lipid droplets throughout the depth of the cell. Images had a 61 μs pixel dwell time, consisted of 512 x 512 pixels, and were averaged 10 times to enhance quality.

Immunofluorescence

RCM-1 embryonic stem cells were tested with antibodies of Oct-4. Differentiated hepatocytes were tested with antibodies of human serum albumin (HSA, Abcam), and HNF4a (Insight Biotechnology). Cells were then washed with PBS, fixed for 20 min with 4% paraformaldehyde in PBS, rinsed with PBS (pH 7.4), then permeabilized with ethanol, and washed with PBS. Cells were blocked with 1% fish gelatin and 0.1% Tween-20 in TBS, then incubated with primary antibodies at 2 μg/ml in blocking solution. Samples were washed with 0.1% Tween-20 in TBS, then incubated in blocking solution with a secondary antibody (Invitrogen) conjugated to the fluorophore Alexa-488. Cells were washed with PBS, then incubated with DAPI, and finally washed with PBS. All items were sourced from Sigma unless otherwise stated. Immunofluorescence images are reproduced in Fig. S7. Images were acquired on a Zeiss Axioscope 2 microscope, equipped with an AxioCam color CCD camera, and a Plan-Neofluar NA 0.75, 40x phase contrast objective.

Results

Atomic Force Microscopy (AFM)

The AFM tip was indented into 40 different RCM-1 embryonic stem cells and 16 different hepatocytes. We calculated the elasticity (Young's modulus) of each cell – see Fig S1 for details. Histograms of elasticity measurements for both cell types are shown in Fig. 1. The distribution of elasticity values among 40 individual stem cells was found to be 53.1 ± 28.6 kPa, and the distribution of elasticity values among 16 individual hepatocytes was found to be 16.4 ± 6.0 kPa. The two means are different to a highly statistically significant level [$p<0.00001$] as found by Welch's t-test.

In order to distinguish stem cells from their differentiated progeny, a threshold value of elasticity should be applied. With a threshold of 25 kPa (assigning all cells below threshold as hepatocytes, and all those above to be stem cells), it can be deduced from the distributions in Fig. 1 that cell types can be identified with an optimum accuracy of 91%. This corresponds to a sensitivity of 94% for identifying hepatocytes, and a specificity of 90%.

Previous AFM studies have measured the elasticity of RCM-1 embryonic stem cells as mostly in the range 2-8 kPa(16) using a model of a conical AFM tip; and the elasticity of mouse embryonic stem cells as 0.265 kPa(46) which spontaneously differentiated towards a neural lineage of elasticity 0.579 kPa. Liver endothelial cells have an elasticity of ~2 kPa(47) as measured by AFM, and a micropipette study of single hepatocytes found an elasticity of 181 Pa(48). Ultrasound studies of the liver of healthy human volunteers found elasticity values of 620 ± 240 Pa(49) and 640 ± 80 Pa(50), and Magnetic Resonance Elastography found a value of 1.16 ± 0.28 kPa(51). All these values are for tissue *in vivo* rather than our *in vitro* cell culture measurements. Meaningful comparisons between different techniques and models are difficult, as absolute values rely on fitting acquired data to

different models and are subject to systematic errors, but a meaningful comparison between samples is far more likely using the same technique, method and model (as in this article).

Raman Spectroscopy

Raman spectra were acquired on 22 different embryonic stem cells and averaged (blue curve), 22 different fully differentiated hepatocytes (after 17 or 18 days, red curve), and 11 cells which had been differentiated towards hepatocytes for 7 days (green curve). Average spectra from each of these three cell types are plotted in Fig. 2.

Although there are clear differences between average spectra, it is not clear what is the variation from cell to cell, nor would it be clear how to assign a new unknown cell as one of these types. In order to highlight the spectral differences, and reject similarities between all cell types, a statistical analysis is performed on all the spectral data. Principal Component Analysis (PCA)(52) reduces each acquired spectrum to a sum of basis spectra (PC1, PC2, PC3…) with a weighting of each basis set. Each spectrum is rewritten as (α.PC1 + β.PC2 + γ.PC3 +…), so can be reduced to a set of scores (α, β, γ…). PC1 contains the highest variance between spectra, and PC2, PC3… contain decreasing variance.

In Fig. 3 we plot values of the scores of the two most significant principal components PC2 and PC8, for known cell types (stem cells, and 17- or 18-day differentiated hepatocytes). The first 8 principal components are plotted against each other in different graphs, and the one which produces the best separation is selected. Each Raman spectrum has been reduced by PCA to a single data point on the graph. In Fig. 3 we defined clear regions with a line which separates stem cells from fully (17- or 18-day) differentiated hepatocytes with an accuracy of 95.5% (which corresponds to a sensitivity in identifying stem cells from hepatocytes of 100% and a specificity of 92%). In Fig. S3 we achieved an accuracy of 97% in discriminating embryonic stem cells (22 cells) from 7-day differentiated

hepatocytes (11 cells), and in Fig. S4 an accuracy of 100 % is achieved in discriminating 7-day hepatocytes (11 cells) from 17-day hepatocytes (22 cells). A lower accuracy of cell assignment, 91% is found when comparing all 3 groups of cells, in Fig. S5.

In order to extract the chemical differences measured between stem cells and the fully differentiated hepatocytes, we can plot the simple difference between average spectra from Fig. 2. This simple subtracted spectrum (hepatocytes minus stem cells) is plotted in Fig. 4 alongside another difference spectrum which has been calculated only from PC2 and PC8 – the two most significant basis spectra required to separate the two groups. To calculate this spectrum, the average position of data points in Fig. 3 is calculated for both cell types, and their separation in each axis reveals the proportion of each spectrum of PC2 and PC8 into a mixture of these two basis spectra which is termed PCmix. Spectra have been normalized to their highest peak before principal component analysis, so that variations in cell thickness will not dominate the measurements. We want to compare relative biochemistries and avoid differences due to cell size, so should normalize all spectra. Spectra which have not been normalized, show similar features and differences but there is better overlap between normalized spectra.

Analysis of these difference spectra in Fig. 4 reveals several clear biochemical changes, which are listed in Table 1, by comparison with a well-cited Raman spectroscopy database(53). We observe an increase in lipids and some proteins; and a reduction in DNA, amino acids, and other proteins. The high density of lipid droplets within hepatocytes is well known(54,55), so an increase of lipid content is expected during differentiation. The nuclear volume of embryonic stem cells is known to be high compared to the volume of the whole cell(56), so the relative DNA content is expected to decrease during differentiation. For the 7-day differentiated cells, DMSO (at 1% in the media) is visible with peaks at 677 cm^{-1} and 711 cm^{-1}(57).

Dielectrophoresis (DEP)

DEP was performed on 220 stem cells and 85 fully (17- or 18-day) differentiated hepatocytes. A summary of the experimentally measured cell diameters and DEP cross-over frequencies (f_{xo}) for RCM1 embryonic stem cells and their differentiated progeny (hepatocytes) is given in Table 2, together with their membrane capacitances derived using equation [1].

$$C_{mem} = \frac{\sqrt{2}}{2\pi r f_{x0}} \sigma_m \qquad [1]$$

where f_{xo} is the cross-over frequency of the cell, r is radius of cell and σ_m is the conductivity of the suspending medium(58). Measurement of f_{xo} and C_{mem} has been shown to provide a sensitive, minimally-invasive way to monitor changes in cell states associated with activation and clonal expansion, apoptosis, necrosis and responses to chemical and physical agents(59-62). The standard deviation values given are based on approximating the f_{xo} and C_{mem} distributions shown in Fig. 5 as normal distributions as shown in Table 2. The results presented in Table 2 and Fig. 5 give capacitances of 17.4 $\pm$ 4.2 mF/m^2 and 15.3 ± 4.8 mF/m^2 for embryonic stem cells and hepatocytes respectively, with corresponding cross-over frequencies of 70.9 ± 17.7 kHz and 92.2 ± 28.2 kHz. Out of the three variables of size, cross-over frequency and capacitance, the two cell populations (stem cells and hepatocytes) are best separated by their cross-over frequencies. The distribution of these cross-over frequencies is shown in Fig. 5 for the two populations. By using a threshold value of 80 kHz, an optimum accuracy of 72% is achieved, which corresponds to a sensitivity in identifying hepatocytes from stem cells of 75% and a specificity of 65%.

Stimulated Raman scattering (SRS) Microscopy

SRS microscopy was performed at a Raman shift of 2930cm^{-1}, corresponding to the asymmetric stretch frequency for CH_2 groups, which is dominated by lipids in living cells. Fig. 6(a) displays the variation of the concentration of CH_2 groups in embryonic stem cells, which shows the nucleus as

dark, (with bright nucleoli), and the cytoplasm as uniformly bright. The dark nucleus is observed for all eukaryotic cells, as DNA bases contain no CH_2 groups, but the cytoplasm and nucleoli appear brighter as they contains amino acids which do possess CH_2 groups.

Fig. 6(b) is dominated by large numbers of lipid droplets in hepatocytes differentiated for 17 or 18 days. The presence of lipid droplets in hepatocytes is well established(54,55), which are normally imaged with Nile Red or Oil Red stains or fluorescent conjugates such as BODIPY for live cells. SRS microscopy images lipid droplets clearly and rapidly in live cells, without extrinsic labels or cell fixation. The presence of high numbers of lipid droplets compared to the almost complete absence of droplets in the embryonic stem cells, is a clear method to distinguish between these cell types with high accuracy. This SRS imaging method is repeated in Fig. S6. Both sets of SRS images enable far clearer distinguishing between stem cells and hepatocytes, than phase contrast microscopy in Fig. 2.

Immunofluorescence

In order to have confidence that we are indeed comparing embryonic stem cells and hepatocytes, we performed immunofluorescence imaging on these cell types. As well as the observation that embryonic stem cells self-renew and form colonies surrounded by stromal cells, we used the monoclonal antibody Oct-4 to confirm their pluripotency. Fully differentiated hepatocytes did not self-renew, and were tested with antibodies of human serum albumin (HSA), and Hepatocyte Nuclear Factor 4 alpha (HNF4a). Immunofluorescence images are shown in Fig. S7.

Both sample types, namely embryonic stem cells and fully differentiated hepatocytes, were imaged with all three antibodies. The immunofluorescence images in Fig. S7 help confirm both the pluripotency of the RCM-1 cells, and the hepatocyte nature of the fully differentiated cells.

Discussion

In many cases, the use of endogenous labels (such as fluorescent antibodies) to characterize and sort cells is undesirable. This is particularly true for stem cell based therapies where there is a requirement to monitor the pluripotency of cells, and the stage of differentiation, with minimally-invasive techniques. Such quality control is a requirement for tissue engineering and regenerative medicine(63). Although, no cell characterization technique can be said to be completely non-invasive – be it heating from white light imaging, laser exposure with Raman spectroscopy and SRS microscopy, changing culture medium with DEP, or indentation with AFM.

Our Raman spectroscopy results are slow, mainly due to a large focal spot and a strong Raman signal from the substrate, but acquisition times can be improved to up to 10 cells per second(64) for non-adherent cells. Hence a microfluidic device could be used to characterize and sort cells. Optical stretching(65) could be included to measure the mechanical properties, as it has measured the elasticity of cells in under 1 second(65) without issues of sterility in an open AFM arrangement. Speeds would be improved to 10 cells per second, by parallel detection. DEP can also be integrated into such a device(37,66) with conducting electrodes (such as transparent indium tin oxide) in proximity to the cells. DEP cell sorting can be performed on the single cell basis, or to very large numbers of cell simultaneously. Although embryonic stem cells are grown as colonies, splitting into individual cells is not a barrier to subsequent cell culture(67). For adherent cells, Raman spectroscopy, and either sterile AFM or acoustic microscopy(68) (to measure elasticity), could be applied to cell culture to monitor quality on a daily basis. The cell's capacitance as a function of frequency, which for non-adherent cells is measured by DEP, can be measured for adherent cells grown on electrodes and has successfully monitored differentiation of adipose-derived stem cells(69).

Live cells have typical heights of 2 - 10 µm, so our 200 nm indentation by AFM will represent no more than 10% of the cell depth. This maximum 10% rule-of-thumb is advisable to avoid misleading measurements of elasticity. For truly quantitative results, a calibration sample of similar elasticity should be used before measurements with a given cantilever and laser spot position.

A very simple mechanical model of the cell would be a balloon filled an incompressible liquid – the application of pressure distorts the shape of the balloon. A slightly more complex model of mammalian cells would involve a stiff plasma membrane around a liquid cytoplasm with the cytoskeleton providing some stiffness. This in turn contains a nuclear membrane and nucleus, which has an elasticity several times that of the cytoplasm(70-72). Embryonic stem cells contain a very large nucleus, so we would expect to observe a higher value of elasticity than for differentiated hepatocytes, which is indeed what we observe in Fig. 1.

In Raman spectroscopy, no observable photodamage occurred for any of the 55 cells investigated, after illumination with 40 mW of a 785 nm laser for 40 minutes. As this time could be reduced to a matter of seconds per cell by avoiding the use of a substrate(64), the technique can be considered to be minimally-invasive and suitable for repeat measurements.

Considering dielectrophoresis, in Fig. 5 it is clear that embryonic stem cells and fully differentiated hepatocytes both exhibited well-separated distributions of their cross-over frequency (f_{xo}) values [$p<0.00001$], with a decrease in the mean value of 23% when stem cells differentiate into hepatocytes. This cross-over frequency is an experimental value, which depends on a combination of two of the cellular characteristics in equation (1), namely membrane capacitance and cell diameter. The membrane capacitance only shows an increase of 14%, although it is borderline statistically relevant [$p=0.052$], and the cell diameter shows an increase of 10% [$p<0.05$]. The

membrane capacitance itself is inversely proportional to its thickness, and directly proportional to its relative permittivity. There is no information on whether the thickness or the permittivity changes, but a change in the chemical composition will also have an effect on the thickness (for example with different length phospholipids, or with cholesterol content) – the thickness of the membrane cannot change without a change in its chemical composition. Hence we can conclude that there is a significant change in the chemical composition of the membrane.

AFM, DEP and SRS all measure one single variable – elasticity, capacitance, and lipid droplets respectively, so none of these techniques is ideally suited to sorting a large number of different types of cell from each other. Instead, AFM, DEP and SRS are best suited to the characterization of a single cell type, or a mixture of two different cell types or phenotypes. Applied to stem cells, these techniques are most appropriate for monitoring the progress of differentiation to a required cell type. Both start and end states should be calibrated by measuring their elasticity or capacitance. In contrast, Raman spectroscopy effectively measures the presence of a large number of different chemistries – peaks in the spectrum – simultaneously, so is well suited to characterizing or sorting a mixture of several different cell types. The accuracy of each technique will depend on the type of stem cell and differentiated cell. For example there may be little change in membrane capacitance or cytoskeleton between stem cells and their differentiated progeny, in which case DEP and AFM would not be suitable techniques for monitoring that particular differentiation. Raman spectroscopy offers a more general method for distinguishing cell types or phenotypes, although its accuracy will depend on the extent of the change in biomolecular composition. Raman spectroscopy has a proven ability to distinguish different cell phenotypes – for example primary and secondary cancer cells for the same patient and organ(73). In this study we were able to clearly distinguish stem cells from 7-day partially differentiated hepatocytes, and fully differentiated hepatocytes. So it appears to be the most promising technique of the four employed here, for detecting pathological stem cell

differentiation – where differentiation has not occurred to functioning hepatocytes, but to non-functioning hepatocytes or other cell types via spontaneous differentiation.

In conclusion, directed stem cell differentiation has been monitored in a minimally-invasive way with 4 different label-free techniques. Such non-destructive techniques hold particular promise in medicine, whether stem cells are required (in stem cell therapies) or fully differentiated cells are required (as in regenerative medicine and organ replacement). Destructive techniques on the other hand, sample cells from a larger population, so crucially do not measure the remaining surviving cells which are used in therapies. The use of cell surface biomarkers – used in immunofluorescence imaging and flow cytometry – is likely to affect the behavior of living cells, so is best avoided. We have demonstrated the accuracy of label-free techniques with numerical values for AFM (80%), dielectrophoresis (72%), and Raman spectroscopy (95.5%). These individual accuracies compare well with around 88% for comparing two different types of algal cell, using multi-parametric label-free white light cytometry(13). If the mechanical, chemical and capacitive properties are independent, then a weighted combination of AFM, Raman spectroscopy and dielectrophoresis would achieve a combined accuracy of well above the 95.5% achieved for Raman spectroscopy alone.

References

1. Bonner W, Hulett H, Sweet R, Herzenberg L. Fluorescence activated cell sorting. Review of Scientific Instruments 1972;43:404-409.
2. Coons AH, Creech HJ, Jones RN. Immunological Properties of an Antibody Containing a Fluorescent Group. Experimental Biology and Medicine 1941;47:200-202.
3. Handgretinger R, Lang P, Schumm M, Taylor G, Neu S, Koscielnak E, Niethammer D, Klingebiel T. Isolation and transplantation of autologous peripheral CD34+ progenitor cells highly purified by magnetic-activated cell sorting. Bone marrow transplantation 1998;21:987-993.
4. Schmitz B, Radbruch A, Kümmel T, Wickenhauser C, Korb H, Hansmann M, Thiele J, Fischer R. Magnetic activated cell sorting (MACS)—a new immunomagnetic method for megakaryocytic cell isolation: comparison of different separation techniques. European journal of haematology 1994;52:267-275.
5. Oh DJ, Lee GM, Francis K, Palsson BO. Phototoxicity of the fluorescent membrane dyes PKH 2 and PKH 26 on the human hematopoietic KG 1 a progenitor cell line. Cytometry 1999;36:312-318.
6. Matheu MP, Cahalan MD, Parker I. Intravital Imaging of the Immune System. Advances in Intravital Microscopy: Springer; 2014. p 81-103.
7. Gage FH. Cell therapy. Nature 1998;392:18-24.
8. Lindvall O, Kokaia Z, Martinez-Serrano A. Stem cell therapy for human neurodegenerative disorders–how to make it work. 2004.
9. Stummann TC, Bremer S. Embryonic stem cells in safety pharmacology and toxicology. New Technologies for Toxicity Testing: Springer; 2012. p 14-25.
10. Gorba T, Allsopp TE. Pharmacological potential of embryonic stem cells. Pharmacological research 2003;47:269-278.
11. Nussbaum J, Minami E, Laflamme MA, Virag JA, Ware CB, Masino A, Muskheli V, Pabon L, Reinecke H, Murry CE. Transplantation of undifferentiated murine embryonic stem cells in the heart: teratoma formation and immune response. The FASEB Journal 2007;21:1345-1357.
12. Logothetis CJ, Samuels ML, Trindade A, Johnson DE. The growing teratoma syndrome. Cancer 1982;50:1629-1635.
13. Chen CL, Mahjoubfar A, Tai L-C, Blaby IK, Huang A, Niazi KR, Jalali B. Deep Learning in Label-free Cell Classification. Scientific reports 2016;6.
14. Binnig G, Quate CF, Gerber C. Atomic Force Microscope. Physical Review Letters 1986;56:930-933.
15. Kuznetsova TG, Starodubtseva MN, Yegorenkov NI, Chizhik SA, Zhdanov RI. Atomic force microscopy probing of cell elasticity. Micron 2007;38:824-833.
16. Kiss R, Bock H, Pells S, Canetta E, Adya AK, Moore AJ, De Sousa P, Willoughby NA. Elasticity of human embryonic stem cells as determined by atomic force microscopy. Journal of biomechanical engineering 2011;133:101009.
17. Chen Q, Xiao P, Chen J-N, Cai J-Y, Cai X-F, Ding H, Pan Y-L. AFM studies of cellular mechanics during osteogenic differentiation of human amniotic fluid-derived stem cells. Analytical Sciences 2010;26:1033-1037.
18. Titushkin I, Cho M. Modulation of cellular mechanics during osteogenic differentiation of human mesenchymal stem cells. Biophysical journal 2007;93:3693-3702.
19. Raman CV, Krishnan KS. A new type of secondary radiation. Nature 1928;121:501-502.
20. Krafft C, Steiner G, Beleites C, Salzer R. Disease recognition by infrared and Raman spectroscopy. Journal of biophotonics 2009;2:13-28.

21. Chan JW, Taylor DS, Zwerdling T, Lane SM, Ihara K, Huser T. Micro-Raman spectroscopy detects individual neoplastic and normal hematopoietic cells. Biophysical journal 2006;90:648-656.
22. Downes A, Mouras R, Elfick A. Optical spectroscopy for noninvasive monitoring of stem cell differentiation. BioMed Research International 2010;2010.
23. Aksoy C, Severcan F. Role of vibrational spectroscopy in stem cell research. Journal of Spectroscopy 2012;27:167-184.
24. Downes A, Mouras R, Bagnaninchi P, Elfick A. Raman spectroscopy and CARS microscopy of stem cells and their derivatives. Journal of Raman Spectroscopy 2011;42:1864-1870.
25. Chan JW, Lieu DK, Huser T, Li RA. Label-free separation of human embryonic stem cells and their cardiac derivatives using Raman spectroscopy. Analytical chemistry 2009;81:1324-1331.
26. Schulze HG, Konorov SO, Caron NJ, Piret JM, Blades MW, Turner RF. Assessing differentiation status of human embryonic stem cells noninvasively using Raman microspectroscopy. Analytical chemistry 2010;82:5020-5027.
27. Pascut FC, Kalra S, George V, Welch N, Denning C, Notingher I. Non-invasive label-free monitoring the cardiac differentiation of human embryonic stem cells in-vitro by Raman spectroscopy. Biochimica et Biophysica Acta (BBA)-General Subjects 2013;1830:3517-3524.
28. Zumbusch A, Holtom GR, Xie XS. Three-dimensional vibrational imaging by coherent anti-Stokes Raman scattering. Physical Review Letters 1999;82:4142-4145.
29. Evans CL, Potma EO, Puoris'haag M, Côté D, Lin CP, Xie XS. Chemical imaging of tissue in vivo with video-rate coherent anti-Stokes Raman scattering microscopy. Proceedings of the National Academy of Sciences of the United States of America 2005;102:16807-16812.
30. Freudiger CW, Min W, Saar BG, Lu S, Holtom GR, He C, Tsai JC, Kang JX, Xie XS. Label-Free Biomedical Imaging with High Sensitivity by Stimulated Raman Scattering Microscopy. Science 2008;322:1857-1861.
31. Saar BG, Freudiger CW, Reichman J, Stanley CM, Holtom GR, Xie XS. Video-rate molecular imaging in vivo with stimulated Raman scattering. Science 2010;330:1368-1370.
32. Mouras R, Bagnaninchi PO, Downes AR, Elfick AP. Label-free assessment of adipose-derived stem cell differentiation using coherent anti-Stokes Raman scattering and multiphoton microscopy. Journal of biomedical optics 2012;17:116011-116011.
33. Pethig R, Menachery A, Pells S, De Sousa P. Dielectrophoresis: a review of applications for stem cell research. BioMed Research International 2010;2010.
34. Stephens M, Talary M, Pethig R, Burnett AK, Mills KI. The dielectrophoresis enrichment of CD34+ cells from peripheral blood stem cell harvests. Bone marrow transplantation 1996;18:777-782.
35. Velugotla S, Pells S, Mjoseng HK, Duffy CR, Smith S, De Sousa P, Pethig R. Dielectrophoresis based discrimination of human embryonic stem cells from differentiating derivatives. Biomicrofluidics 2012;6:044113.
36. Flanagan LA, Lu J, Wang L, Marchenko SA, Jeon NL, Lee AP, Monuki ES. Unique dielectric properties distinguish stem cells and their differentiated progeny. Stem cells 2008;26:656-665.
37. Muratore M, Srsen V, Waterfall M, Downes A, Pethig R. Biomarker-free dielectrophoretic sorting of differentiating myoblast multipotent progenitor cells and their membrane analysis by Raman spectroscopy. Biomicrofluidics 2012;6:034113.
38. Caralt M. Present and Future of Regenerative Medicine: Liver Transplantation. Transplantation Proceedings 2015;47:2377-2379.

39. Reed J, Walczak WJ, Petzold ON, Gimzewski JK. In situ mechanical interferometry of matrigel films. Langmuir 2008;25:36-39.
40. Garitaonandia I, Amir H, Boscolo FS, Wambua GK, Schultheisz HL, Sabatini K, Morey R, Waltz S, Wang Y-C, Tran H. Increased risk of genetic and epigenetic instability in human embryonic stem cells associated with specific culture conditions. PloS one 2015;10:e0118307.
41. Hay DC, Fletcher J, Payne C, Terrace JD, Gallagher RC, Snoeys J, Black JR, Wojtacha D, Samuel K, Hannoun Z. Highly efficient differentiation of hESCs to functional hepatic endoderm requires ActivinA and Wnt3a signaling. Proceedings of the National Academy of Sciences 2008;105:12301-12306.
42. Trickey WR, Baaijens FP, Laursen TA, Alexopoulos LG, Guilak F. Determination of the Poisson's ratio of the cell: recovery properties of chondrocytes after release from complete micropipette aspiration. Journal of biomechanics 2006;39:78-87.
43. Schulze HG, Foist RB, Okuda K, Ivanov A, Turner RF. A small-window moving average-based fully automated baseline estimation method for Raman spectra. Applied spectroscopy 2012;66:757-764.
44. Schulze HG, Turner RF. A Fast, Automated, Polynomial-Based Cosmic Ray Spike-Removal Method for the High-Throughput Processing of Raman Spectra. Applied spectroscopy 2013;67:457-462.
45. Downes A, Mouras R, Elfick A. A versatile CARS microscope for biological imaging. Journal of Raman Spectroscopy 2009;40:757-762.
46. Pillarisetti A, Desai JP, Ladjal H, Schiffmacher A, Ferreira A, Keefer CL. Mechanical phenotyping of mouse embryonic stem cells: increase in stiffness with differentiation. Cellular Reprogramming (Formerly" Cloning and Stem Cells") 2011;13:371-380.
47. Braet F, Rotsch C, Wisse E, Radmacher M. Comparison of fixed and living liver endothelial cells by atomic force microscopy. Applied Physics A: Materials Science & Processing 1998;66:S575-S578.
48. Wu Z-Z, Zhang G, Long M, Wang H-B, Song G-B, Cai S-X. Comparison of the viscoelastic properties of normal hepatocytes and hepatocellular carcinoma cells under cytoskeletal perturbation. Biorheology 2000;37:279-290.
49. Chen EJ, Novakofski J, Jenkins WK, O'Brien W. Young's modulus measurements of soft tissues with application to elasticity imaging. Ultrasonics, Ferroelectrics, and Frequency Control, IEEE Transactions on 1996;43:191-194.
50. Yeh W-C, Li P-C, Jeng Y-M, Hsu H-C, Kuo P-L, Li M-L, Yang P-M, Lee PH. Elastic modulus measurements of human liver and correlation with pathology. Ultrasound in medicine & biology 2002;28:467-474.
51. Asbach P, Klatt D, Hamhaber U, Braun J, Somasundaram R, Hamm B, Sack I. Assessment of liver viscoelasticity using multifrequency MR elastography. Magnetic Resonance in Medicine 2008;60:373-379.
52. Ringnér M. What is principal component analysis? Nature biotechnology 2008;26:303-304.
53. Movasaghi Z, Rehman S, Rehman IU. Raman spectroscopy of biological tissues. Applied Spectroscopy Reviews 2007;42:493-541.
54. Wang H, Quiroga AD, Lehner R. Analysis of lipid droplets in hepatocytes. Methods in cell biology 2012;116:107-127.
55. Majzner K, Kochan K, Kachamakova-Trojanowska N, Maslak E, Chlopicki S, Baranska M. Raman imaging providing insights into chemical composition of lipid droplets of different size and origin: in hepatocytes and endothelium. Analytical chemistry 2014;86:6666-6674.
56. Sathananthan H, Pera M, Trounson A. The fine structure of human embryonic stem cells. Reproductive biomedicine online 2002;4:56-61.

57. Caspers PJ, Williams AC, Carter EA, Edwards HG, Barry BW, Bruining HA, Puppels GJ. Monitoring the penetration enhancer dimethyl sulfoxide in human stratum corneum in vivo by confocal Raman spectroscopy. Pharmaceutical research 2002;19:1577-1580.
58. Pethig R. Review article—dielectrophoresis: status of the theory, technology, and applications. Biomicrofluidics 2010;4:022811.
59. Wang X, Becker FF, Gascoyne PR. Membrane dielectric changes indicate induced apoptosis in HL-60 cells more sensitively than surface phosphatidylserine expression or DNA fragmentation. Biochimica et Biophysica Acta (BBA)-Biomembranes 2002;1564:412-420.
60. Pethig R, Bressler V, Carswell‐Crumpton C, Chen Y, Foster‐Haje L, García‐Ojeda ME, Lee RS, Lock GM, Talary MS, Tate KM. Dielectrophoretic studies of the activation of human T lymphocytes using a newly developed cell profiling system. Electrophoresis 2002;23:2057-2063.
61. Pethig R, Talary M. Dielectrophoretic detection of membrane morphology changes in Jurkat T-cells undergoing etoposide-induced apoptosis. Iet Nanobiotechnology 2007;1:2-9.
62. Sabuncu AC, Zhuang J, Kolb JF, Beskok A. Microfluidic impedance spectroscopy as a tool for quantitative biology and biotechnology. Biomicrofluidics 2012;6:034103.
63. Berthiaume F, Maguire TJ, Yarmush ML. Tissue Engineering and Regenerative Medicine: History, Progress, and Challenges. Annual Review of Chemical and Biomolecular Engineering 2011;2:403-430.
64. Pascut FC, Goh HT, George V, Denning C, Notingher I. Toward label-free Raman-activated cell sorting of cardiomyocytes derived from human embryonic stem cells. Journal of biomedical optics 2011;16:045002-045002-4.
65. Sraj I, Eggleton CD, Jimenez R, Hoover E, Squier J, Chichester J, Marr DW. Cell deformation cytometry using diode-bar optical stretchers. Journal of biomedical optics 2010;15:047010-047010-7.
66. Hu X, Bessette PH, Qian J, Meinhart CD, Daugherty PS, Soh HT. Marker-specific sorting of rare cells using dielectrophoresis. Proceedings of the National Academy of Sciences of the United States of America 2005;102:15757-15761.
67. Chen KG, Mallon BS, Hamilton RS, Kozhich OA, Park K, Hoeppner DJ, Robey PG, McKay RD. Non-colony type monolayer culture of human embryonic stem cells. Stem cell research 2012;9:237-248.
68. Weiss EC, Anastasiadis P, Pilarczyk G, Lemor RM, Zinin PV. Mechanical properties of single cells by high-frequency time-resolved acoustic microscopy. Ultrasonics, Ferroelectrics, and Frequency Control, IEEE Transactions on 2007;54:2257-2271.
69. Bagnaninchi PO, Drummond N. Real-time label-free monitoring of adipose-derived stem cell differentiation with electric cell-substrate impedance sensing. Proceedings of the National Academy of Sciences 2011;108:6462-6467.
70. Caille N, Thoumine O, Tardy Y, Meister J-J. Contribution of the nucleus to the mechanical properties of endothelial cells. Journal of biomechanics 2002;35:177-187.
71. Dong C, Skalak R, Sung K. Cytoplasmic rheology of passive neutrophils. Biorheology 1990;28:557-567.
72. Guilak F, Tedrow JR, Burgkart R. Viscoelastic properties of the cell nucleus. Biochemical and biophysical research communications 2000;269:781-786.
73. Tsikritsis D, Richmond S, Stewart P, Elfick A, Downes A. Label-free identification and characterization of living human primary and secondary tumour cells. Analyst 2015;140:5162-5168.

Figures

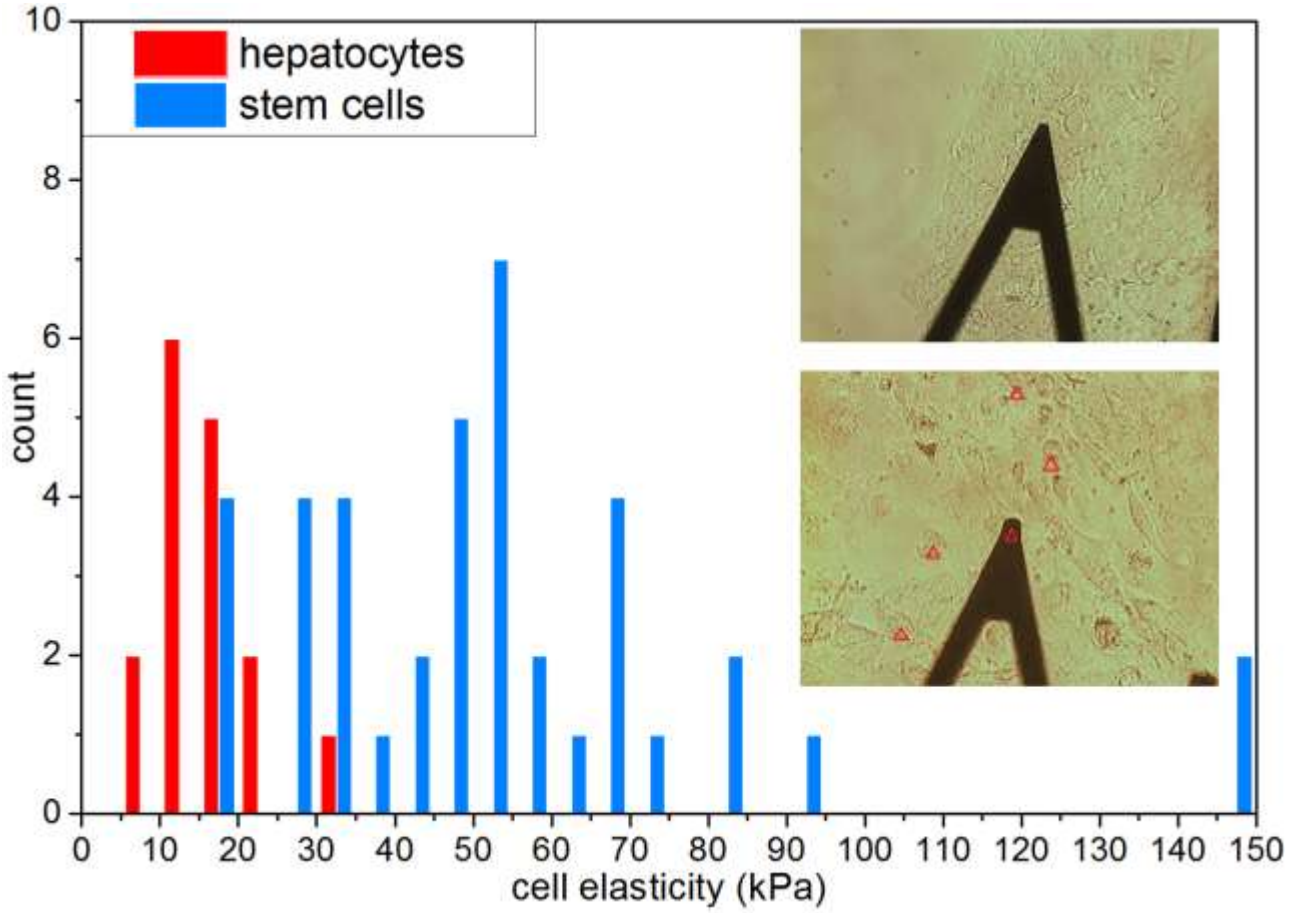

Fig. 1. Histogram of atomic force microscope (AFM) measurements of cell elasticity on 40 RCM-1 embryonic stem cells, and 16 hepatocytes fully differentiated from the RCM-1 embryonic stem cells. Inset are phase contrast images (360 x 270 µm) of the triangular AFM cantilever (stem cells on top, hepatocytes below, with red arrows indicating some measurement positions). Histogram bins are set to a width of 5 kPa, and a value of 25 kPa can be used to define the threshold below which a cell can be assigned as a hepatocyte (and above which can be assigned as a stem cell) with an accuracy of 91%.

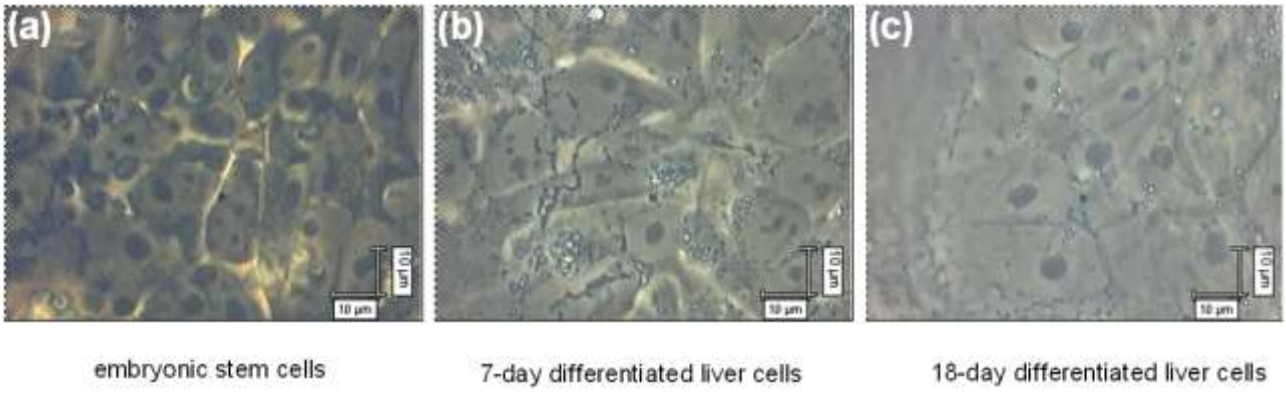

(d)

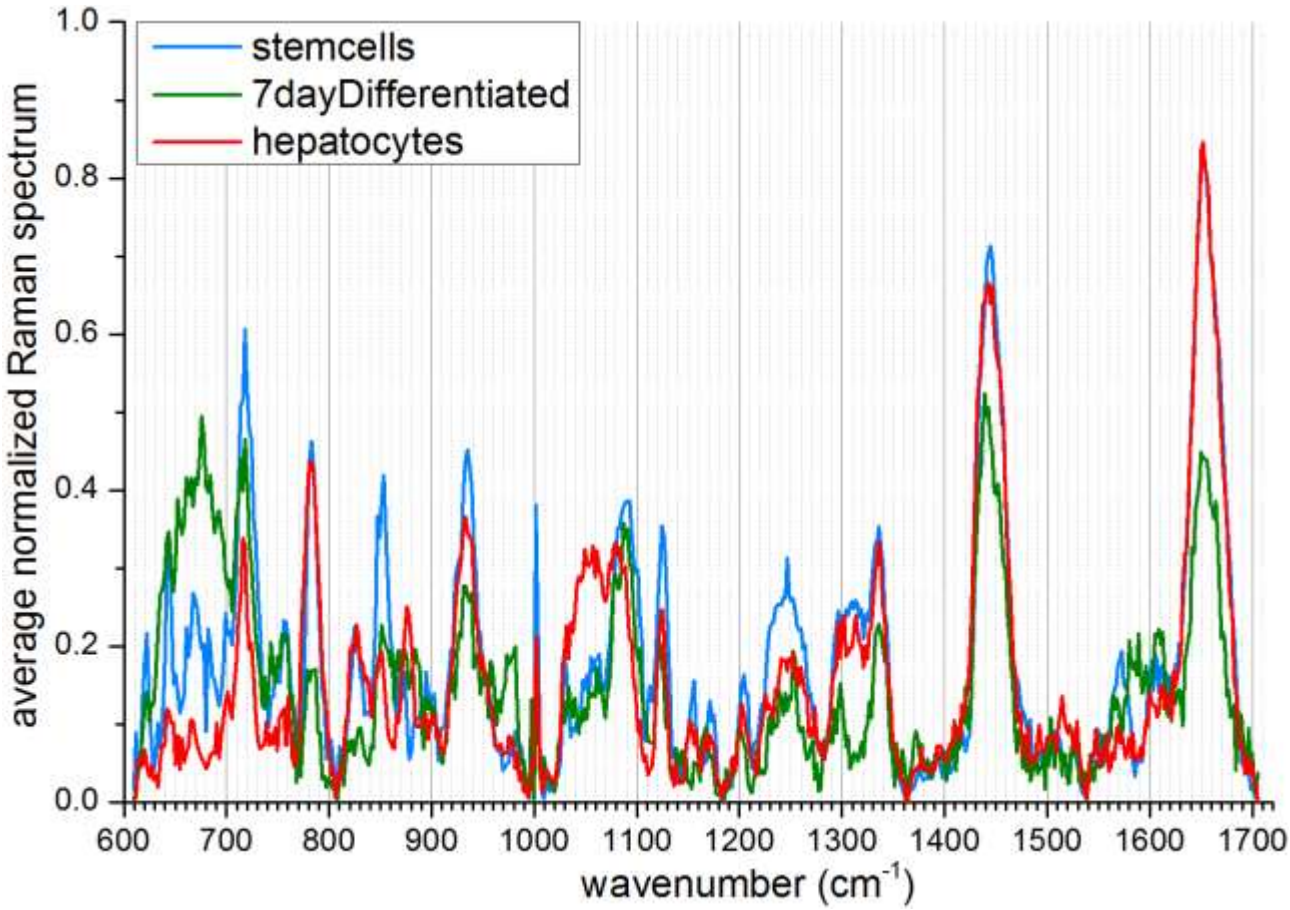

Fig. 2. Phase contrast images of (a) RCM-1 embryonic stem cells, and their progeny (b) 7-day semi-differentiated hepatocytes, and (c) 17-day fully differentiated hepatocytes. (d) The corresponding average Raman spectra for embryonic stem cells (blue curve), hepatocytes differentiated fully for 17 or 18 days (red curve), and hepatocytes differentiated for 7 days (green curve).

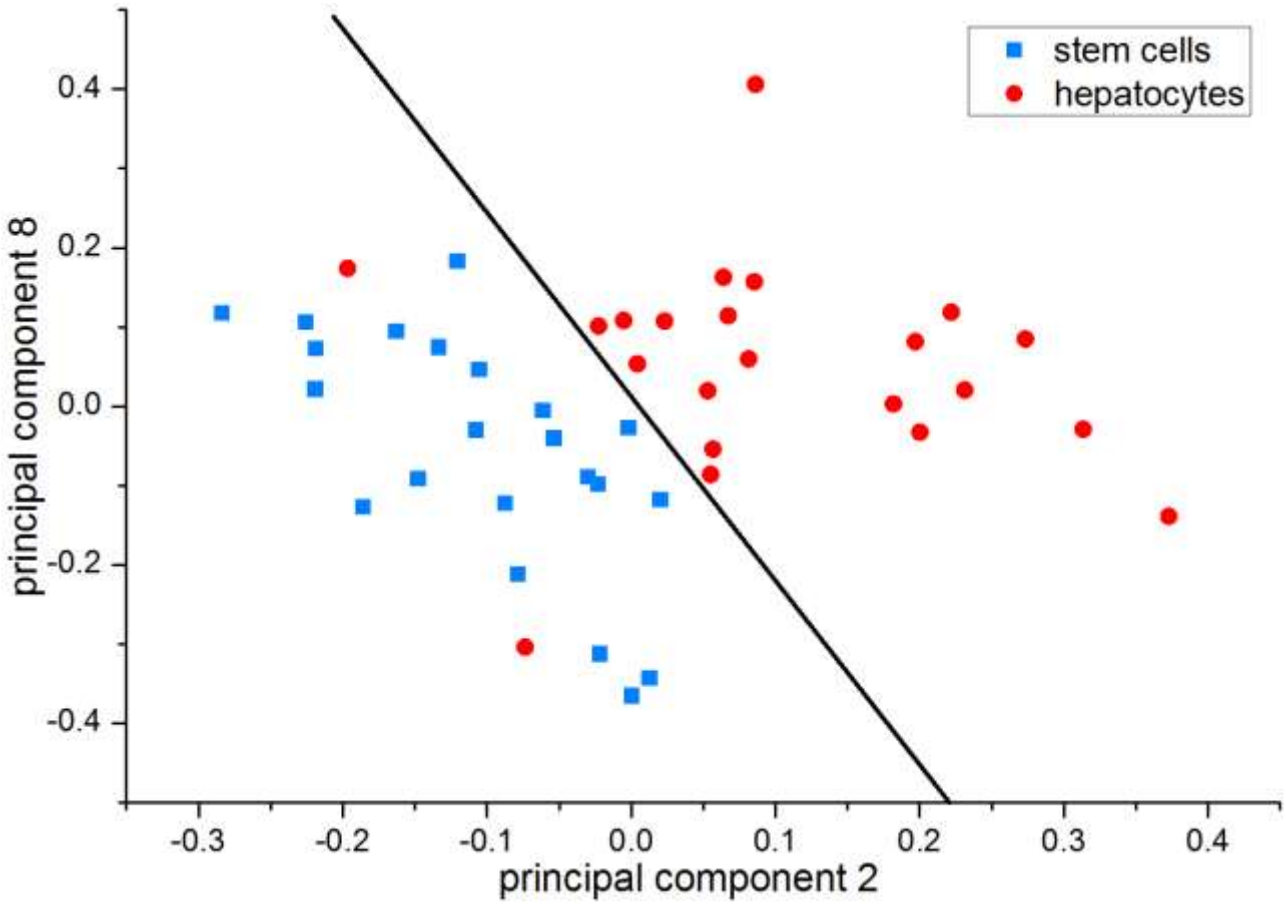

Fig. 3. Principal component analysis (PCA) scatter plots for Raman spectra of 22 embryonic stem cells (blue) and 22 hepatocytes fully differentiated for 17 or 18 days (red). 42 out of 44 cells are on the correct side of the dividing line – so are classified correctly, corresponding to an accuracy of 95.5%.

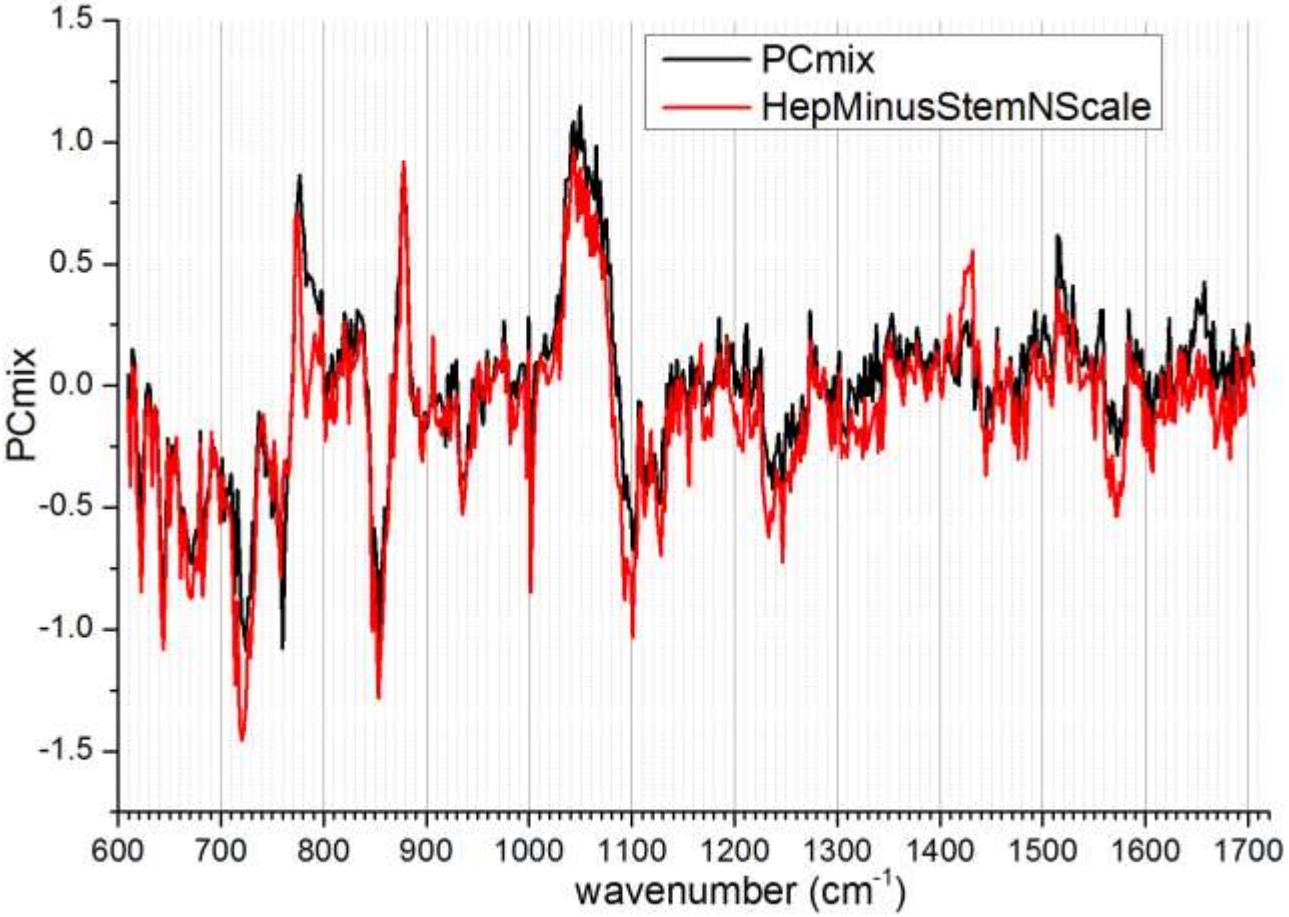

Fig. 4. Differences between Raman spectra from embryonic stem cells and fully (17- or 18-day) differentiated hepatocytes. The red curve is the simple subtraction between average spectra from Fig 2. The black curve represents the difference between the same two groups, but only using the two basis spectra PC2 and PC8.

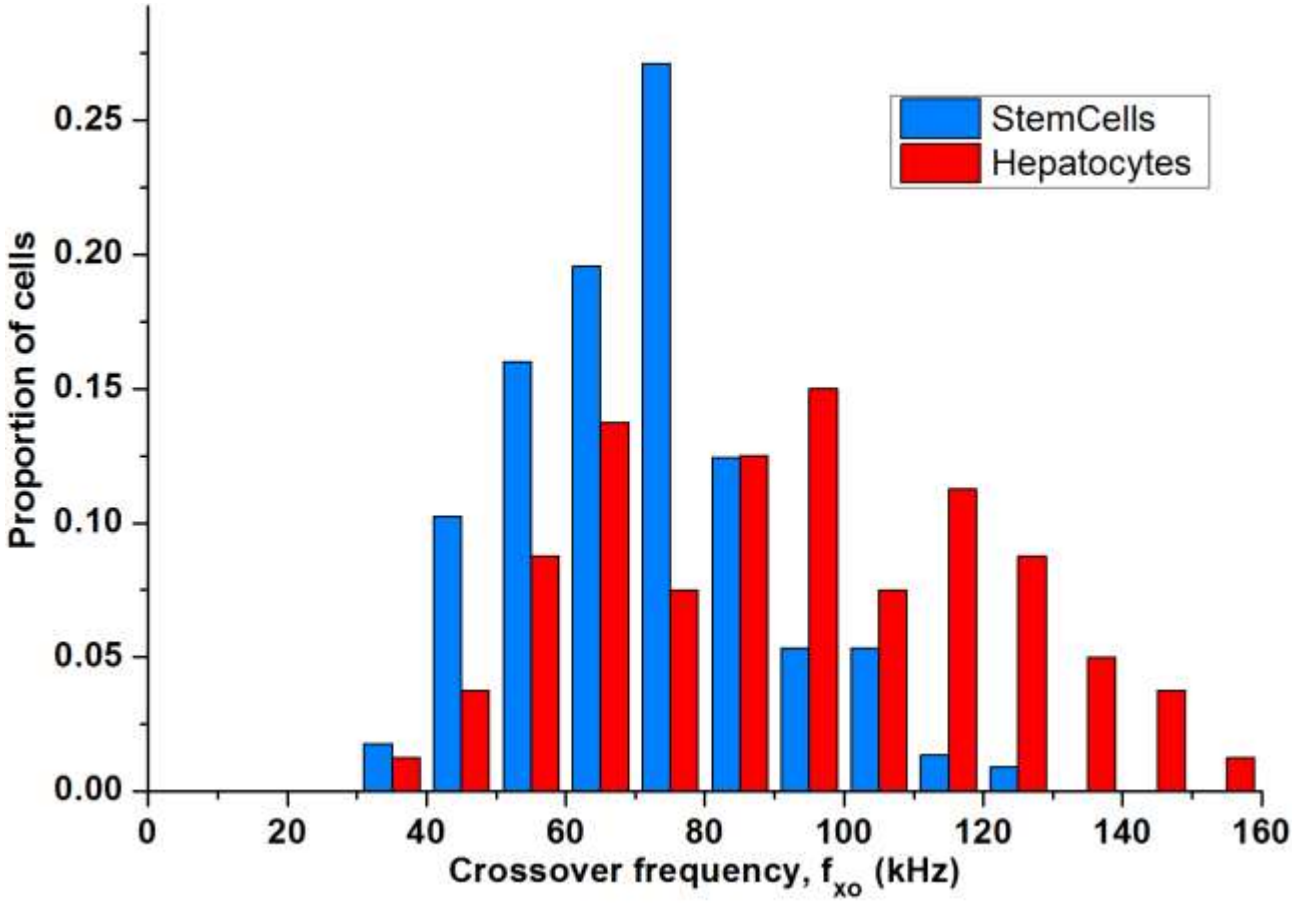

Fig. 5. Probability distributions of the Dielectrophoresis (DEP) cross-over frequencies (f_{xo}) measured for embryonic stem cells in blue, and fully (17- or 18-day) differentiated hepatocytes in red.

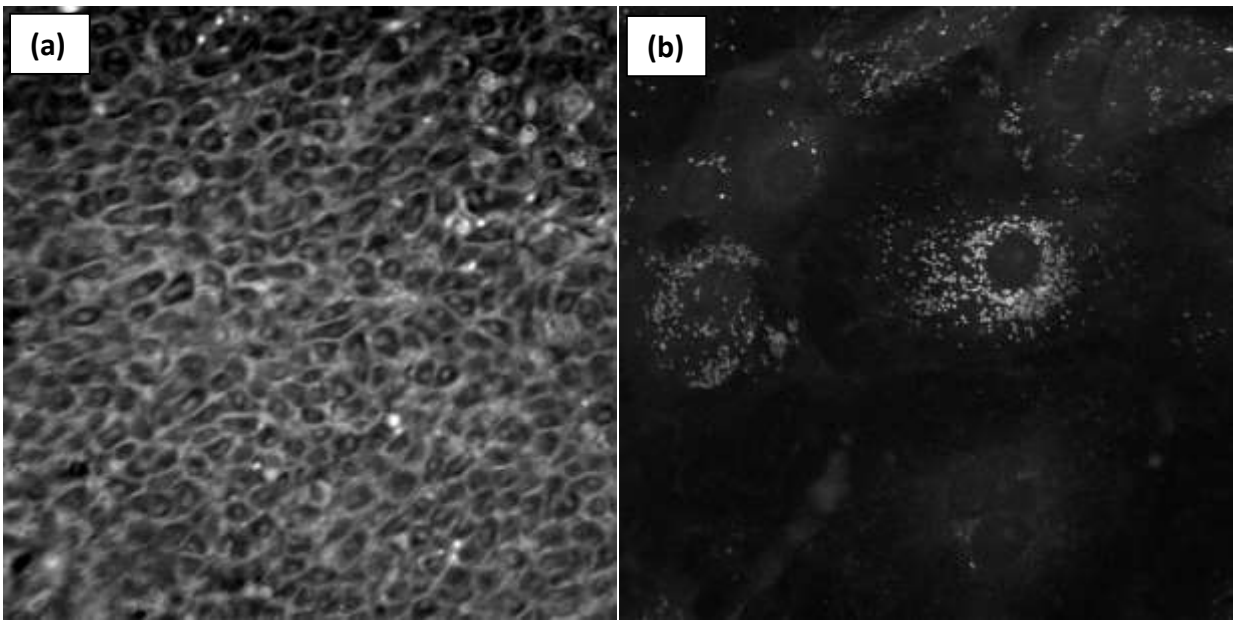

Fig. 6. Stimulated Raman Scattering images at 2930 cm^{-1}, of (a) RCM-1 embryonic stem cells, and (b) 18-day differentiated hepatocytes (maximum intensity Z-projection over a 10 µm stack to highlight all lipid droplets). Image sizes are 200 µm, and laser powers at the sample are 30 mW of 811.3 nm and 30 mW of 1064.4 nm.

Raman frequency (wavenumbers, cm^{-1})	*Biomolecular assignment*	*Variation from stem cells to hepatocytes*
621	phenylalanine (amino acid)	decrease
643	phenylalanine, tyrosine (amino acids)	decrease
677, 711	dimethyl sulphoxide (DMSO)	same
720-722	DNA	decrease
785-788	DNA/RNA	decrease
811	RNA	decrease
826	DNA	decrease
854	tyrosine (amino acid)	decrease
877	lipids	increase
928-940	proline, valine (amino acid)	decrease
1003	phenylalanine (amino acid)	decrease
1032, 1057	lipids	increase
1093	PO^{2-} (DNA)	decrease
1126, 1156	proteins	decrease
1208	phenylalanine (amino acid)	decrease
1224, 1242	β-sheet proteins	increase
1301	lipids	increase
1339	lipids	increase
1421	DNA / RNA	decrease
1437-1453	lipids (CH_2 deformation)	increase
1573-1578	G,A (DNA bases)	decrease
1640-1680	amide I (proteins)	increase

Table 1**:** Assignment of biochemical species relating to peaks in Raman spectra in Fig. 4.

Cell Type	Diameter (μm)	f_{XO} (kHz)	C_{mem} (mF/m^2)
RCM1 (n=225)	12.8±1.6	70.9±17.7	17.4±4.2
Hepatocytes (n=80)	11.6±1.4	92.2±28.2	15.3±4.8

Table 2**:** Summary of dielectrophoresis data: cell diameter, DEP cross-over frequency (f_{XO}) and membrane capacitance (C_{mem}) – obtained for human embryonic stem cells (RCM-1) and their fully differentiated progeny (hepatocytes).

Supporting information

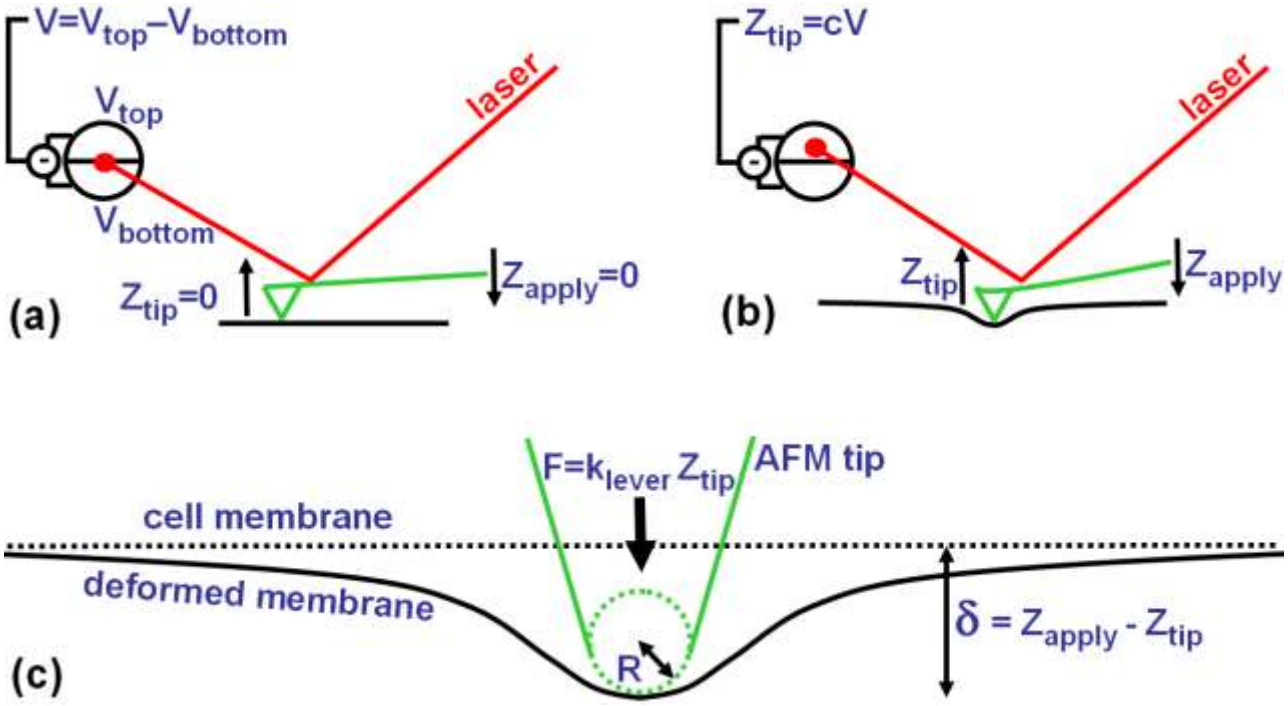

Fig. S1. Schematic diagrams of atomic force microscope (AFM) mechanical measurements. (a) The green AFM cantilever is brought into contact with a hard glass surface, and no net force deflects the cantilever. (b) The fixed end of the cantilever is indented into a soft surface by a distance Z_{apply}, and the free end bends upwards by a distance Z_{tip} (relative to the fixed end). The cantilever deflection is measured by the movement of the reflected laser spot on a split photodiode. (c) A zoom of the contact between the end of the AFM tip and cell membrane. The indentation δ, caused by a force F, is calculated as the difference between the known Z_{apply} and measured Z_{tip}. To fit AFM data, values of F are offset so that the first recorded value is zero, and values of F are smoothed over 10 points with respect to Z_{apply}. The indentation δ is calculated as $\delta = Z_{apply} - F/k_{lever}$, where k_{lever} is the cantilever stiffness. The indentation point is defined as the lowest value above which all values of F are positive, where δ is offset to zero. The first points of this curve is now (0,0) and the last point is (F_{max},δ_{max}). The elasticity, E is calculated for $F=F_{max}$ and $\delta=\delta_{max}$ from the Hertz model, $F = 4/3.(E.R^{1/2}.\delta^{3/2}) / (1-\nu^2)$ where ν is Poisson's ratio = 0.37 for biological tissues (43).

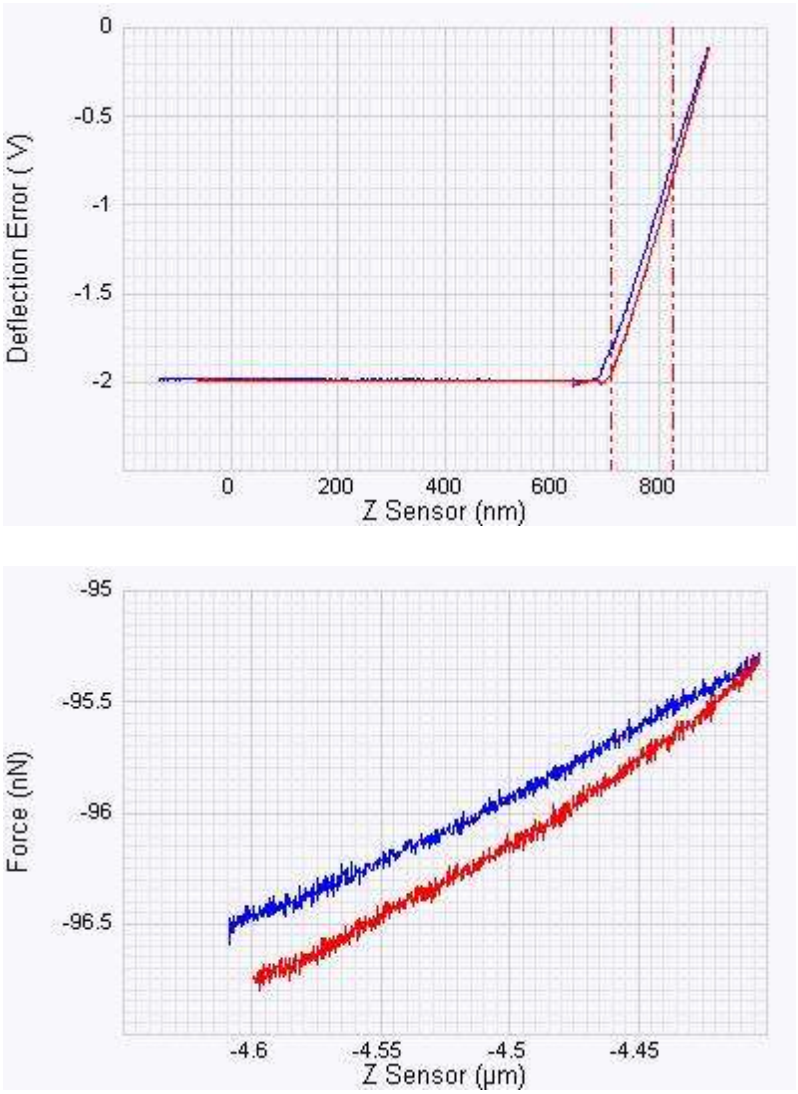

Fig. S2. Top: a representative force-distance curve on a glass surface (blue is the indentation ramp, red is the retraction). The left part of the trace is the cantilever approaching the glass, then a hard contact occurs. The gradient of the straight line is the used to calibrate the split photodiode from Volts to nanometres. Bottom: a representative force-distance curve on a stem cell. Curves follow a dependence of $\delta^{3/2}$ (Hertz sphere model) rather than δ^2 (Hertz cone model) indicating that a sphere-on-plane model is a more appropriate than a cone-on-plane (Sneddon) model.

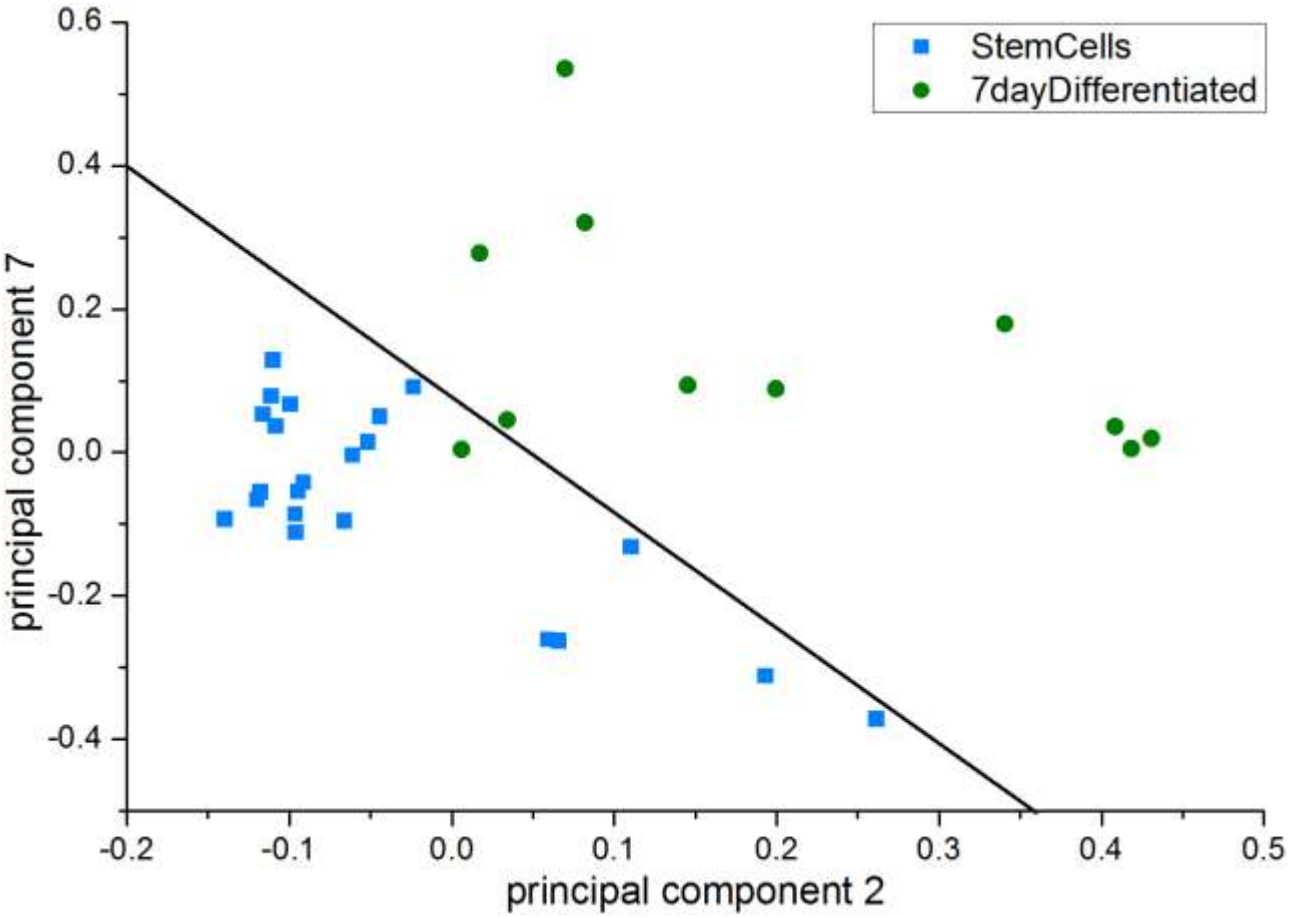

Fig. S3. Principal component analysis (PCA) scatter plots for Raman spectra of 22 embryonic stem cells (blue squares) and 11 cells differentiated from stem cells toward hepatocytes for 7 days (green circles). 32 out of 33 cells are on the correct side of the dividing line – so are classified correctly, corresponding to an accuracy of 97%.

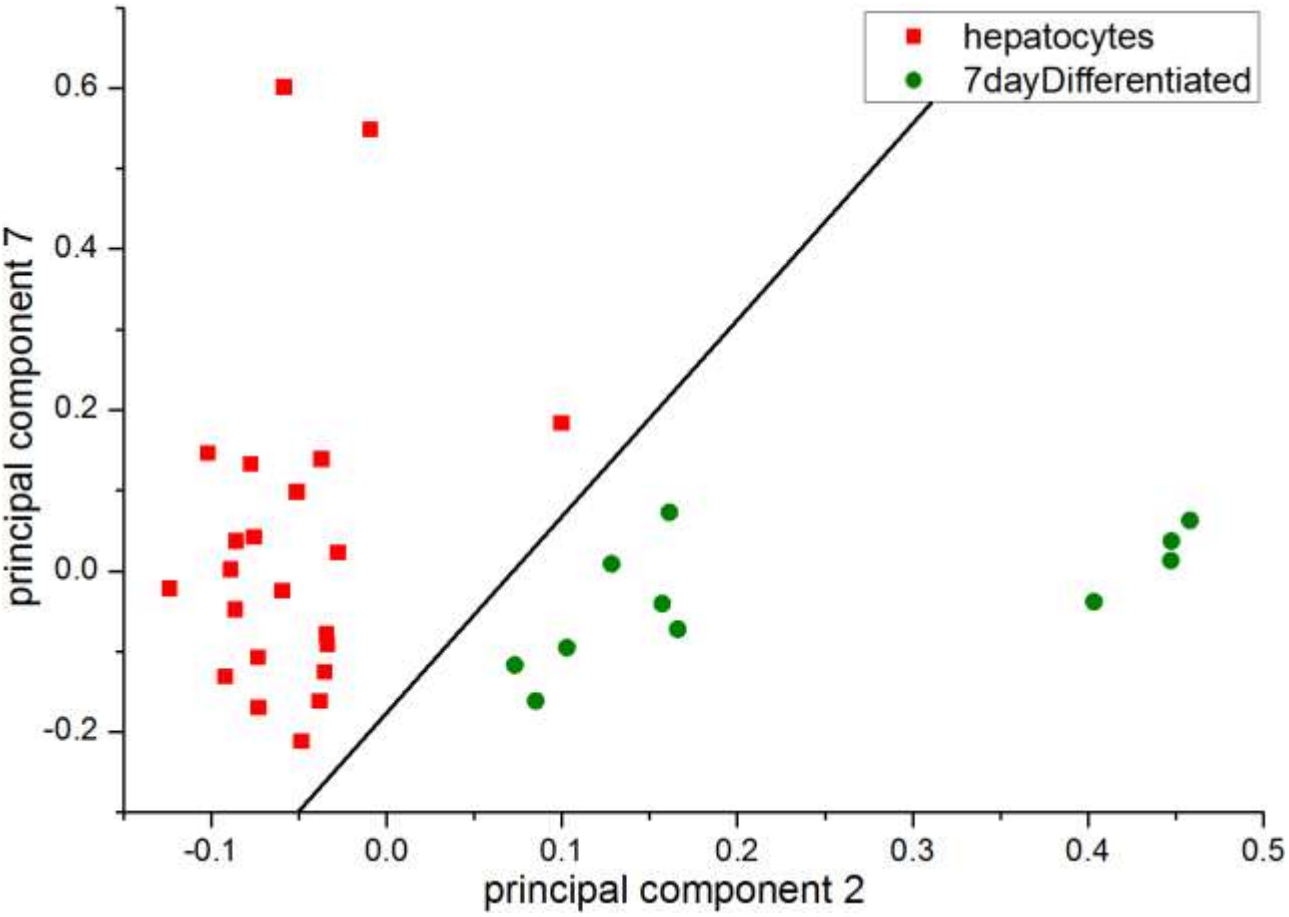

Fig. S4. Principal component analysis (PCA) scatter plots for Raman spectra of 22 fully differentiated hepatocytes (red squares) and 11 cells differentiated from stem cells toward hepatocytes for 7 days (green circles). All 33 cells are on the correct side of the dividing line – so are classified correctly, corresponding to an accuracy of 100%.

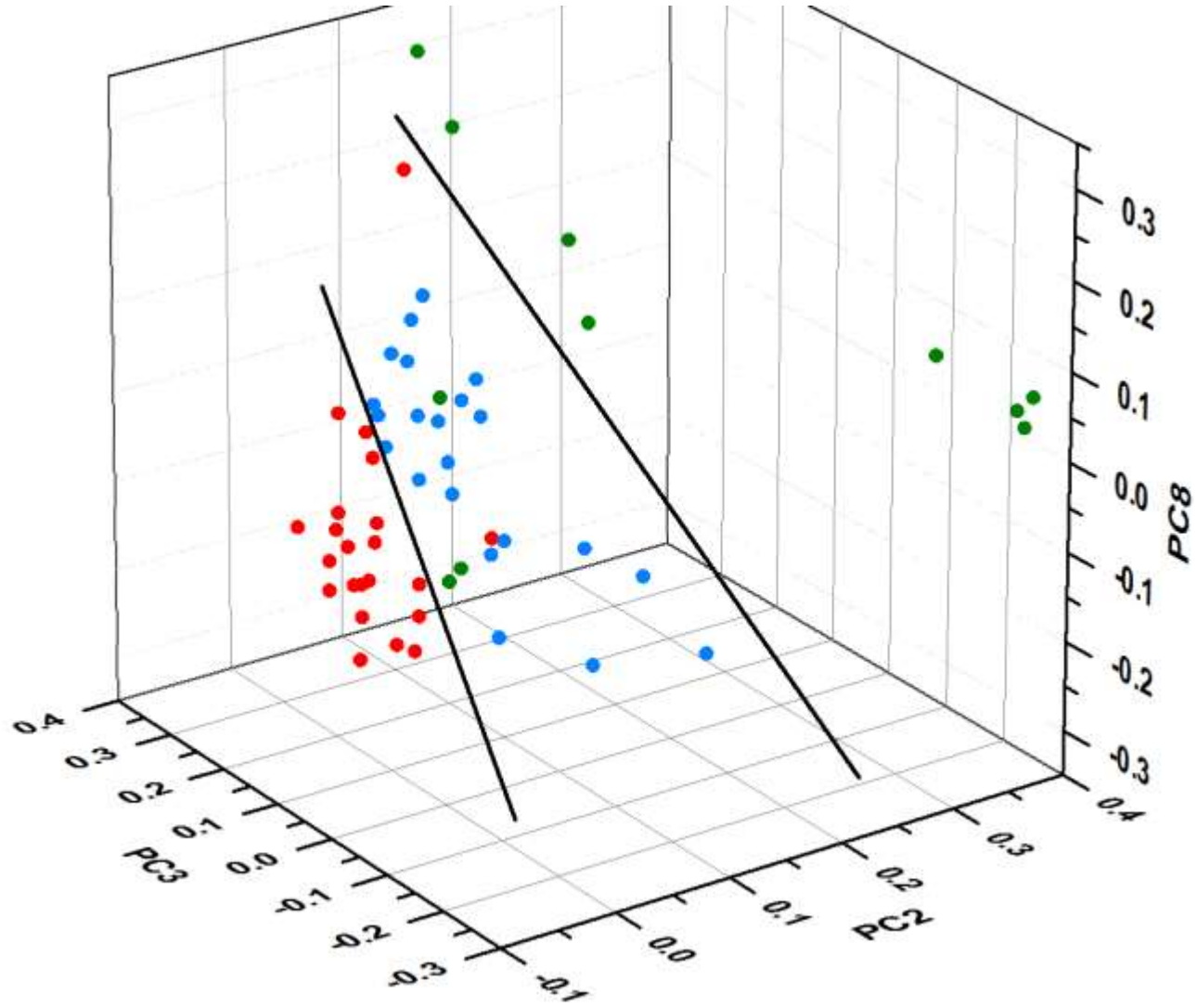

Fig. S5. Principal Component Analysis (PCA) 3D scatter plot of Raman spectra for all groups (stem cells in blue, 7-day differentiated hepatocytes in green, and fully differentiated hepatocytes in red). When planes are added to delineate regions (visible as lines in the image, as the viewing direction is contained within both planes), an accuracy of assignment of cell type of 91% (50/55 cells) is achieved.

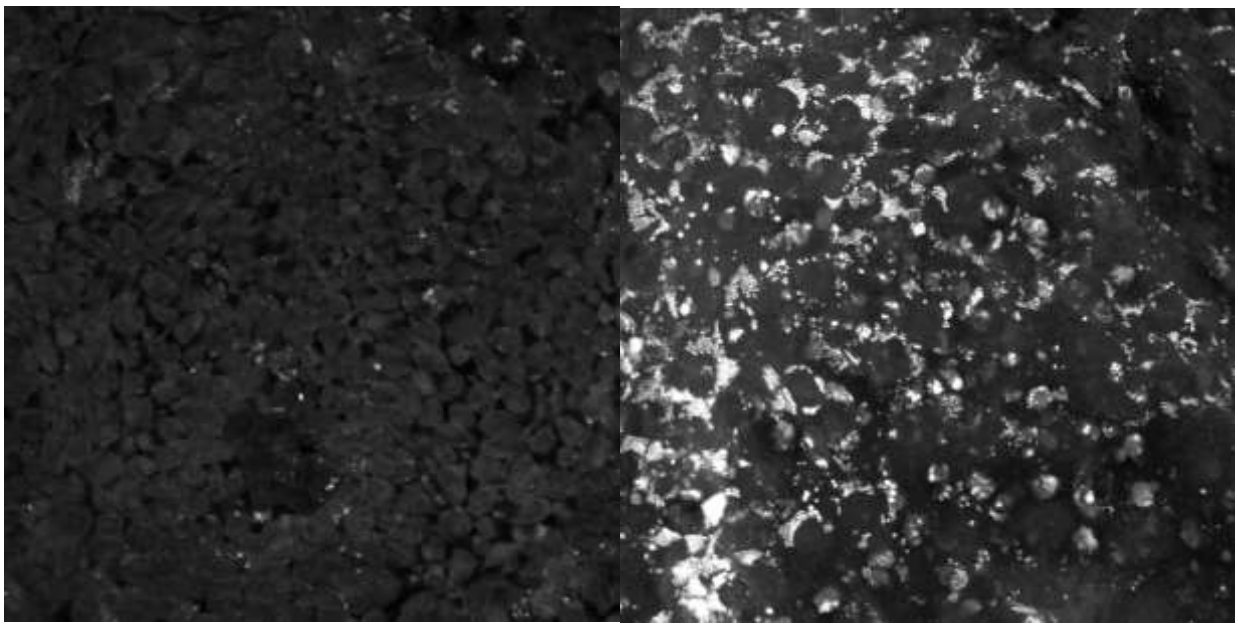

(a) **(b)**

Fig. S6. Further stimulated Raman scattering (SRS) microscopy images at 2930 cm^{-1}, of (a) RCM-1 embryonic stem cells, and (b) 17-day differentiated hepatocytes (maximum intensity Z-projection over a 10 μm high stack to highlight lipid droplets). Image sizes are 200 μm, and laser powers at the sample are 30 mW of 811.3 nm and 30 mW of 1064.4 nm.

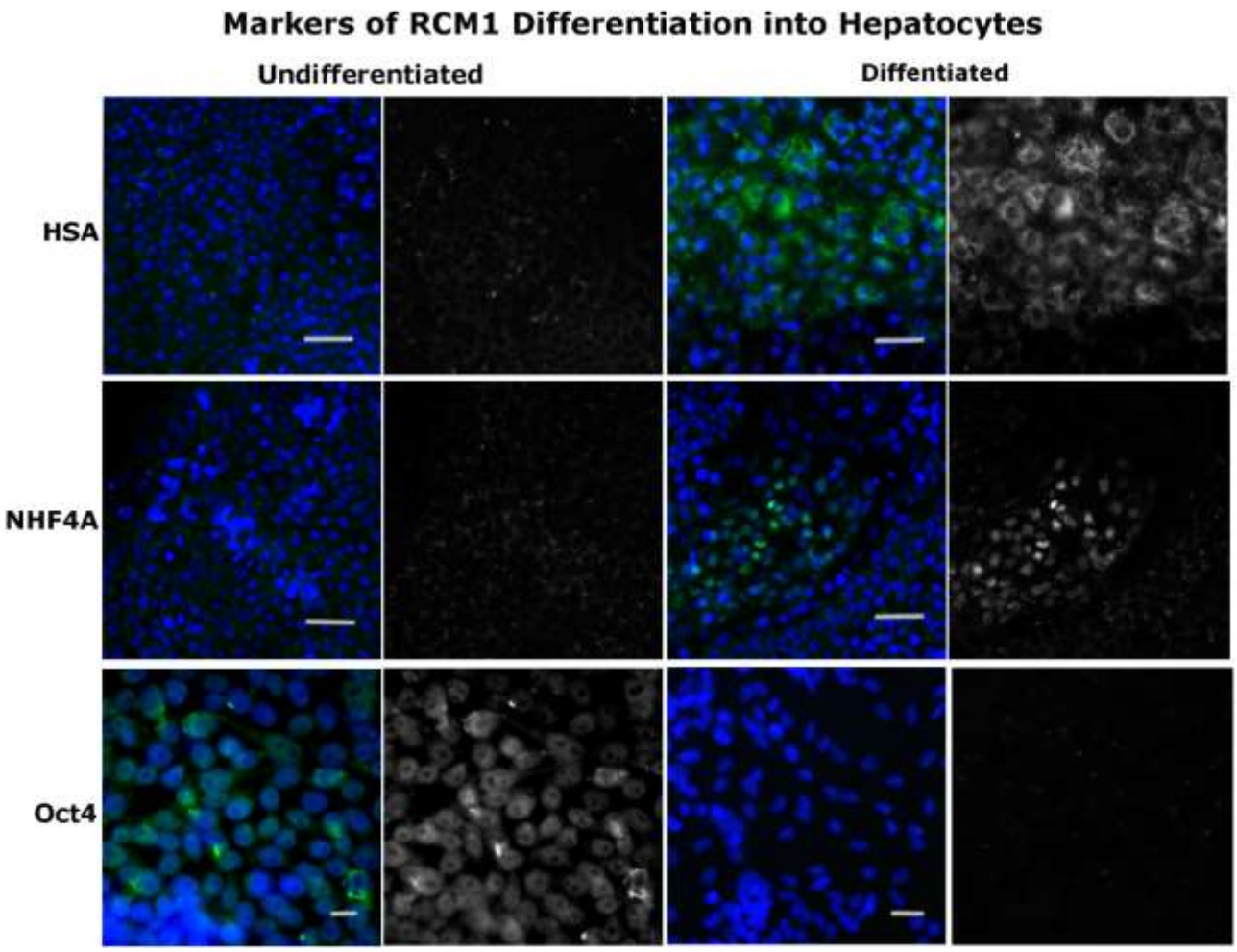

Fig. S7. Immunofluorescence images of (left:) undifferentiated embryonic stem cells (RCM-1), and (right:) cells differentiated for 17 days into hepatocytes. Both cell types were immunostained (green) for two markers known to be strongly expressed in hepatocytes, human serum albumin (HSA) and hepatocyte nuclear factor 4 alpha (HNF4A); and for one marker known to be strongly expressed in embryonic stem cells, octamer-binding transcription factor 4 (Oct4). Both cell types were counterstained with DNA stain DAPI. For clarity, these green channels are reproduced in greyscale images in the second and fourth columns. Scale bars represent 20 µm (all HSA and HNF4a images), 5 µm (Oct-4 undifferentiated), and 10 µm (Oct-4 differentiated). Embryonic stem cells were also strongly proliferating (requiring passaging every 3-4 days), but differentiated hepatocytes did not proliferate.